RSC Advances

PAPER

View Article Online
View Journal | View Issue

Cite this: *RSC Adv.*, 2023, **13**, 15634

Porous silicon decorated with Au/TiO_2 nanocomposites for efficient photoinduced enhanced Raman spectroscopy†

Sheng-Yang Huang,[a] Wei-Ning Gao,[b] Chia-Man Chou*[acd] and Vincent K. S. Hsiao *[b]

Received 19th April 2023
Accepted 19th May 2023

DOI: 10.1039/d3ra02598e

rsc.li/rsc-advances

In this study, we investigated the potential of porous silicon (PSi) modified with Au/TiO_2 nanocomposites (NCPs) as a substrate for photoinduced enhanced Raman spectroscopy (PIERS). One-step pulsed laser-induced photolysis (PLIP) was used to embed Au/TiO_2 NCPs in the surface of PSi. Scanning electron microscopy revealed that adding TiO_2 nanoparticles (NPs) during PLIP led to the formation of predominantly spherical Au NPs with a diameter of approximately 20 nm. Furthermore, modifying the PSi substrate with Au/TiO_2 NCPs considerably enhanced the Raman signal of rhodamine 6G (R6G) after 4 h of ultraviolet (UV) irradiation. Real-time monitoring of the Raman signals of R6G at different concentrations under UV irradiation revealed that the amplitude of the signals increased with the irradiation time for R6G concentrations ranging from 10^{-3} M to 10^{-5} M. PSi substrates decorated with Au/TiO_2 NCPs may be used to develop materials for PIERS applications.

1. Introduction

Surface-enhanced Raman spectroscopy (SERS) is a highly sensitive surface sensing technique extensively used for detecting biomarkers[1] and organic chemicals, such as pesticides.[2] Studies have reported 10-fold to 100-fold signal enhancement and the detection of individual molecules.[3] The surface enhancement of Raman spectra was first observed in the 1970s in the presence of rough metallic surfaces.[4] Although the origin of SERS enhancement is unknown, it is partially attributed to the generation of electromagnetic field resonance near a molecule, referred to as surface plasmon or localized surface plasmon resonance.[5] In this phenomenon, the electron clouds of nanoparticles (NPs) collectively oscillate under excitation by incident light, resulting in nanoscale Raman signal enhancement.[6] Therefore, most recent SERS-related studies have focused on using metallic NPs.[7–10] Raman surface enhancement is also attributed to a chemical effect in which a molecule binds to a metallic NP and the charge transfer (CT) between the molecule and the NP is promoted.[11]

Parkin *et al.* developed a photoinduced enhanced Raman spectroscopy (PIERS) technique.[12] They used Ag and Au NPs in combination with TiO_2 NPs to fabricate a metal NP/TiO_2 nanocomposite (NCP) as a SERS substrate for detecting the Raman spectra of target molecules. The main difference between SERS and PIERS is that PIERS needs UV light irradiating the SERS substrate. The Raman signal was notably amplified when the substrate was exposed to UV light before Raman analysis. PIERS relies only on UV irradiation, eliminating the need for additional procedures and simplifying the preparation of the substrate. With PIERS, Raman signals can be amplified several tens of times, enabling superior performance to that of SERS.[13] Currently, PIERS can be performed using one of three methods: exposing the SERS substrate to UV light and subsequently adding the target molecules to the substrate for Raman analysis; adding the target molecules to the substrate and subsequently exposing it to UV light for analysis; or simultaneously irradiating the measuring point in real time with the laser and a UV light source placed near the laser source.

Several studies have demonstrated the advantages of PIERS over SERS, including a wider detection range for small molecules, such as explosives,[13] pollutants,[14] peptide,[15] and traces of organic dyes.[16] PIERS can also detect small molecules with small Raman scattering cross-sections.[17] The compatibility with both visible and blue light is another advantage of PIERS over SERS, which is limited to the deep UV range. Furthermore, PIERS substrates are not limited to noble metal NP-decorated semiconductor materials; transition metal oxides, transition metal dichlorides, organic semiconductor heterostructures, and NPs decorated with insulating substrates can also be used

[a]*Division of Pediatric Surgery, Department of Surgery, Taichung Veterans General Hospital, Taichung 407219, Taiwan. E-mail: cmchou@mail.vghtc.gov.tw*

[b]*Department of Applied Materials and Optoelectronic Engineering, National Chi Nan University, Nantou 54561, Taiwan. E-mail: kshsiao@ncnu.edu.tw*

[c]*School of Medicine, College of Medicine, National Yang Ming Chiao Tung University, Taipei 112304, Taiwan*

[d]*Department of Post-Baccalaureate Medicine, College of Medicine, National Chung Hsing University, Taichung 402202, Taiwan*

† Electronic supplementary information (ESI) available. See DOI: https://doi.org/10.1039/d3ra02598e

as PIERS substrates.[13] Despite the advantages of PIERS, several challenges must be overcome. First, the preparation and conditions of the PIERS substrate must be optimized for consistency and simplicity. Second, light source characteristics, such as wavelength, intensity, exposure time, and exposure conditions, are critical to PIERS performance and should be optimized. Lastly, the sensitivity and specificity of PIERS for biological analysis should be explored and increased through the improvement of substrate materials and control of experimental conditions.

According to Parkin *et al.*, Raman signals are enhanced in PIERS because of the formation of oxygen vacancies in noble metal and metal oxide interfaces. When a Au–TiO_2 NCP substrate is irradiated with UV light, the O_2 and H_2O molecules adsorbed on the substrate react with the UV light, forming oxygen vacancies on the TiO_2 surface.[12] The charge on the Au NP–decorated surface increases when the Au–TiO_2 substrate is irradiated with a 633 nm Raman laser, resulting in PIERS enhancement. However, the enhancement effect gradually diminishes with the neutralization of the oxygen vacancies by positively charged ions in the air. Once the oxygen vacancies have been eliminated, the enhancement effect dissipates, but it can be generated again through UV irradiation. Thus, the formation of oxygen vacancies is a reasonable explanation for photoinduced Raman enhancement. Some researchers have proposed alternative methods for photoinduced enhancement because generating oxygen vacancies through UV irradiation is challenging with many semiconductor materials. Rice *et al.* have suggested that photoinduced enhancement results from charge separation and migration within semiconductors.[15] When a sample is irradiated with UV light, free electrons are excited and migrate from the valence band to the conduction band and are then can be transferred to, for example, Ag NPs on the semiconductor surface, further enhancing the Raman scattering signal of analytes in contact with such NPs. Liu *et al.* observed notable enhancement of Raman signals in heterogeneous Ag–TiO_2 nanowire arrays;[14] the heterojunction effectively separated electrons and holes, and UV light excited the electrons in the valence bands of both rutile and anatase TiO_2, causing them to migrate to the conduction band. The anatase TiO_2 accepted photoelectrons from rutile TiO_2, considerably increasing the electron density on the surface and further enhancing scattering signals. The aforementioned studies enhanced Raman signals through three mechanisms: a chemical mechanism (CM) involving enhanced CT, CT between the semiconductor and metal NPs, and an electromagnetic mechanism (EM) involving electron accumulation in or release by NPs. The CM and EM enhance signals simultaneously, aided by the CT between the semiconductor and metal NPs. Optical parameters, such as absorption spectra, can be measured before and after light exposure to test the enhancement effect.[13]

On the basis of the literature, a Au–TiO_2 NCP system was selected as the PIERS material in the present study. Au-coated glass is often used as a substrate for SERS owing to the nanoscale pits and peaks on its surface that create "hot spots"; however, this material is expensive. Therefore, we used porous silicon (PSi)[18–25] as the substrate, which can provide "hot spots" and support the Au–TiO_2 NCPs. The Au–TiO_2 NCPs were fabricated through one-step pulsed laser-induced photolysis (PLIP).[26] Scanning electron microscopy (SEM) revealed the Au NPs grown on the surface of the PSi substrate to exhibit various shapes, including circles, triangles, and hexagons, and sizes ranging from tens to hundreds of nanometers when TiO_2 NPs were not added to the precursor during PLIP. By contrast, the Au NPs grown on the surface of the PSi substrate with the TiO_2 NPs added to the precursor were predominantly spherical and much smaller, with diameters of approximately 20 nm. We speculate that the addition of TiO_2 NPs during PLIP fabrication affected the surface energy of the PSi, resulting in smaller and predominantly spherical Au NPs. These findings indicate that PSi substrates modified with Au–TiO_2 NCPs can significantly enhance the Raman signals of rhodamine 6G (R6G) dye exposed to UV light irradiation for 4 h. Thus, we investigated the real-time changes in the Raman signals of various concentrations of R6G under UV irradiation. The experimental results indicated that the R6G Raman signal intensity increases with the duration of UV irradiation for R6G concentrations ranging from 10^{-3} M to 10^{-5} M. However, at 10^{-6} M, UV irradiation could not enhance the R6G Raman signal, indicating that our Au/TiO_2 NCP-decorated PSi for use as a PIERS substrate should be further improved. Nevertheless, the as-prepared material may have applications in optoelectronic devices and provide insight into the future development of Au/TiO_2 NCP-decorated PSi materials.

2. Experimental

2.1 Fabrication of porous silicon (PSi)

PSi samples were prepared through the room-temperature wet electrochemical etching of a p-type, B-doped, one-side-polished Si wafer with a thickness of 525 ± 25 μm and a resistivity of 1–10 Ω cm, oriented in the ⟨100⟩ direction. 2 × 2 cm^2 p-type Si samples were placed in lab-made Teflon cells, with a piece of Cu foil serving as the back working electrode and a small O-ring used to adhere the PSi samples to the cells (Fig. 1a). The area exposed to the etching solution was approximately 0.8 cm^2, and

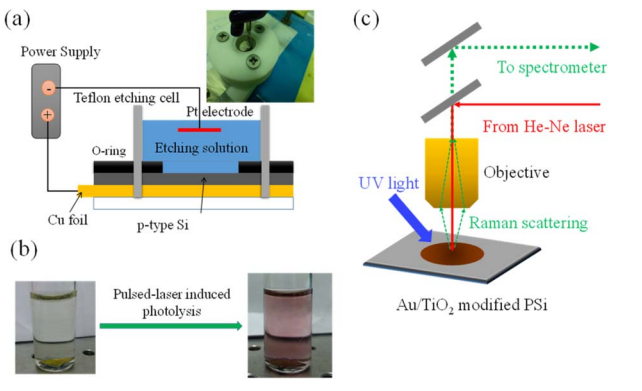

Fig. 1 (a) Schematic and image of PSi substrate fabrication through electrochemical etching. (b) Images of precursor containing $HAuCl_4$, H_2O_2, and TiO_2 NPs before and after PLIP. (c) Schematic of PIERS using a micro-Raman system and UV light source.

a constant current density of 50 mA cm^{-2} was applied for 20 min. The etching solution was composed of hydrofluoric acid (48–51% in water, Acros Organics), isopropyl alcohol (99.5%, Shimakyu), and deionized (DI) water in a 1 : 2 : 1 volume ratio. A Pt disk (0.6 cm^2) was immersed in the solution as a counter electrode. No other chemical or thermal treatment was conducted after etching. The cells and samples were then washed with ethanol and dried under a stream of nitrogen.

2.2 Pulsed-laser induced photolysis (PLIP) method

PLIP was used to grow the Au NPs on the PSi.[26] Auric acid ($HAuCl_4$) can be used as a precursor and photodecomposing agent to obtain Au^{3+}. This ion is later reduced by the photon, and Au NPs are generated under high-energy pulsed laser. Because of the unique properties of ultra-short pulse duration and ultra-high peak power intensity, the PLIP technique is considered a clean and prompt technique to reduce metal ions into NPs without using any other chemical reagent. Here, one PSi substrate was placed inside a glass vial containing a solution composed of 15 mL of 0.33 mM $HAuCl_4$ and 6 mL of 10 mM H_2O_2, and another was placed in a vial containing a solution of 15 mL of 0.33 mM $HAuCl_4$, 6 mL of 10 mM H_2O_2, and an additional 0.001 mg of TiO_2 NPs (5 nm, iNNO) in 2 mL of DI water. The mixed aqueous solutions were irradiated using a Nd:YAG nanosecond pulsed laser operating at 532 nm and 47 mJ for 10 min. The images of the aqueous solution before and after laser irradiation in Fig. 1b indicate a pronounced color change from light yellow to light red. The color change resulted from the formation of the Au NPs or Au–TiO_2 NCPs.

2.3 Photoinduced enhanced Raman spectroscopy (PIERS) method

Raman measurement was performed using a micro-Raman system consisting of a spectrometer with a 15 mW, 633 nm He–Ne laser and a 40× objective lens, as shown in Fig. 1c. The studied analyte, rhodamine 6G (Aldrich), was prepared in ethanol and diluted in different concentration. The PIERS sample was prepared by directly dropped the analyte onto the PSi sample. The Raman signal was collected within 5 s. The *in situ* Raman signals were measured by irradiating the substrate with a 100 mW UV LED light at different time interval.

2.4 Materials characteristics

Surface morphology and elemental analysis of PSi were performed by scanning electron microscopy (SEM) and energy-dispersive X-ray spectroscopy (EDS) method using a JEOL JSM-7800 F field-emission scanning electron microscope (JEOL, Tokyo, Japan). X-ray diffraction (XRD) patterns of Au–TiO_2 decorated PSi was obtained in the 2θ range of 0–90° on a high-resolution X-ray diffractometer (Bruker AXS GmbH, Karlsruhe, Germany). The morphology and particle size of the Au NPs and Au–TiO_2 NCPs were investigated through transmission electron microscopy (TEM) using a JEM-2100 transmission electron microscope (JEOL, Tokyo, Japan).

3. Results and discussion

Previous study utilized a method wherein O_2 and H_2O were adsorbed on Au/TiO_2 and irradiated with UV light to form oxygen vacancies after 4 h of UV preirradiation.[12] In the present study, the Au NPs and Au/TiO_2 NCPs were first grown on the surface of the same PSi sample through PLIP. Then, a 10^{-3} M rhodamine 6G (R6G) aqueous solution was dropped onto the PSi sample surface. As in the previous method, after the solution evaporated, the two PSi samples (Au NP-coated and Au–TiO_2 NCP-coated PSi) were irradiated with UV light for 4 h. The resulting Raman spectra were compared and are shown in Fig. 2. The R6G Raman spectrum of the PSi sample with TiO_2 NPs added through PLIP exhibited notable enhancement after exposure to UV irradiation for 4 h. By contrast, the R6G Raman spectrum of the PSi sample without TiO_2 was not enhanced after the same duration of UV irradiation. Thus, PIERS substrates can be fabricated through the addition of TiO_2 through PLIP to PSi fabricated through electrochemical etching.

To determine the effect of adding TiO_2 NPs to the precursor through PLIP observe the nanomaterials and surface structures of the PSi, SEM was performed on PSi obtained through PLIP with precursors with and without additional TiO_2 NPs. Fig. 3a shows the surface morphology of the PSi sample fabricated through PLIP without additional TiO_2 in the precursor. NPs and microparticles of different shapes were observed on the surface of the PSi substrate, including circular NPs with sizes of approximately 100 nm and triangular, hexagonal, and irregularly shaped NPs with sizes of approximately 500 nm. We also

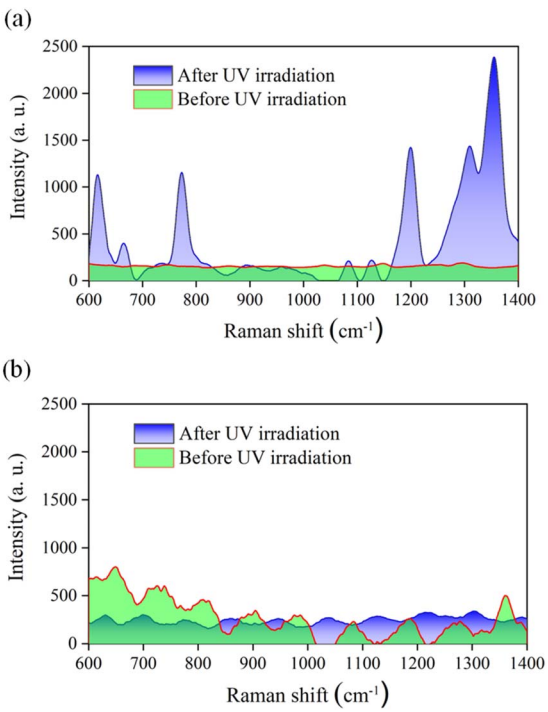

Fig. 2 Raman spectra of R6G (10^{-3} M) on PSi substrates fabricated (a) with and (b) without TiO_2 NPs added to the precursor during PLIP. All Raman spectra were obtained under the same conditions.

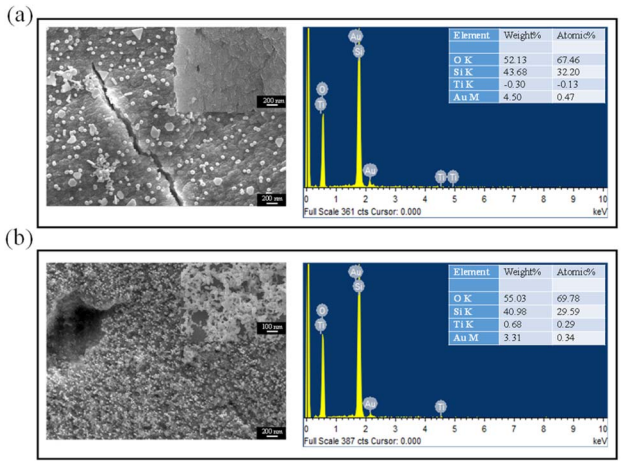

Fig. 3 SEM images and EDS spectra indicating the surface morphologies and composition of PSi samples fabricated (a) without and (b) with TiO_2 NPs in the $HAuCl_4/H_2O_2$ precursor used in PLIP. The inset in (a) was a bare PSi substrate and the inset in (b) was the Au/TiO_2 NCP-modified PSi of higher magnification.

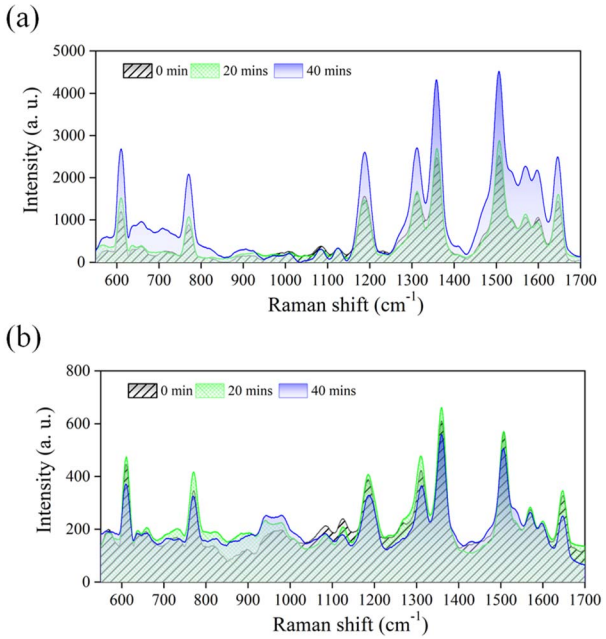

Fig. 4 Raman spectra of R6G (10^{-3} M) for PSi substrates exposed to UV irradiation for different durations and fabricated (a) with and (b) without TiO_2 NPs in the precursor used in the PLIP process. All Raman spectra were obtained under the same conditions.

performed SEM analysis on the bare Psi sample showing no NPs (Fig. 3a inset). Energy-dispersive X-ray spectroscopy (EDS) analysis revealed that these particles were Au NPs and Ti was absent, confirming the addition of no TiO_2 NPs to the $HAuCl_4/H_2O_2$ precursor during PLIP. However, when PLIP was conducted with TiO_2 NPs added to the precursor, the size and shape of the NPs on the surface of the PSi were considerably different. The resulting particles were smaller (approximately 10 nm) and relatively uniform in shape, as illustrated in Fig. 3b. The EDS analysis also revealed the existed Ti elements. The transmission electron microscopy (TEM) also confirmed the addition of TiO_2 helps to fabricate Au NPs with sphere shapes, as shown in Fig. S1.† To provide additional experimental proof of Au–TiO_2 NCPs deposition on PSi, the X-ray diffraction (XRD) analysis was performed on the Au–TiO_2 modified PSi, as shown in Fig. S2.† The typical diffraction peaks at 27.3°, 36.1°, 40.5°, and 66.4° corresponded to the (110), (101), (111), and (002) crystal faces, respectively, of rutile TiO_2.[27] The other peaks at 38.3°, 44.6°, 64.7°, and 77.5° corresponded to the (111), (200), (220), and (311) planes, respectively, of the face-centered cubic Au structure.[28] Therefore, adding TiO_2 NPs to the $HAuCl_4/H_2O_2$ precursor during PLIP may help the growth of homogeneous Au NPs on the surface of PSi.

UV irradiation is crucial in enhancing the Raman signals of PIERS substrates. Previous studies have demonstrated that continuous UV irradiation for 4 h is necessary for signal enhancement.[12] However, this method is not suitable for most analytes with clear Raman signals because of the long irradiation duration, even though it may be suitable for analytes with less clear Raman responses. Therefore, we utilized Au–TiO_2-decorated PSi for real-time UV irradiation and investigated its potential as a PIERS platform for detecting the common analyte R6G. The experimental results are depicted in Fig. 4a. The Au–TiO_2-decorated PSi substrate enhanced the R6G Raman signals (610, 772, 1187, 1310, 1358, 1505, and 1646 cm^{-1}), as compared with those before UV irradiation. After exposure to UV irradiation for 20 min, the characteristic peaks of R6G did not exhibit further enhancement. However, after 40 min of irradiation, the intensities of the R6G characteristic peaks had increased by a factor of 2. When the Au-decorated PSi was used as the PIERS substrate, the R6G Raman spectra were measured under the same micro-Raman conditions, as shown in Fig. 4b. Although the characteristic peaks of R6G were detectable, the Raman signal intensity was only one-tenth of that obtained using the Au–TiO_2-decorated PSi substrate. These results indicate that UV irradiation of the Au-modified PSi for 40 min cannot strengthen the characteristic Raman signals of R6G (an analyte with strong Raman signals) but that Au/TiO_2-modified PSi substrates fabricated through PLIP can enhance such signals after only 40 min of UV irradiation for high analyte concentrations (10^{-3} M).

Most studies on SERS have focused on the detection limit of substrates. However, we tried to investigate the detection ability of the fabricated Au–TiO_2-decorated PSi as PIERS substrate *in situ* under UV exposure. The results in Fig. 5 indicate that the R6G Raman signal was significantly enhanced after UV irradiation when the R6G concentration was 10^{-4} M. When the R6G concentration was 10^{-5} M, the R6G Raman signal was enhanced by a factor of 2 after 20 minutes of UV irradiation, but prolonging the UV exposure to 40 min did not significantly increase the characteristic peak of the R6G Raman signal. However, some R6G Raman peaks (at 667, 990, and 1573 cm^{-1}) that were not initially visible without UV irradiation were enhanced. When the R6G concentration was 10^{-6} M, the R6G Raman signals were undetectable even after 40 min of UV irradiation.

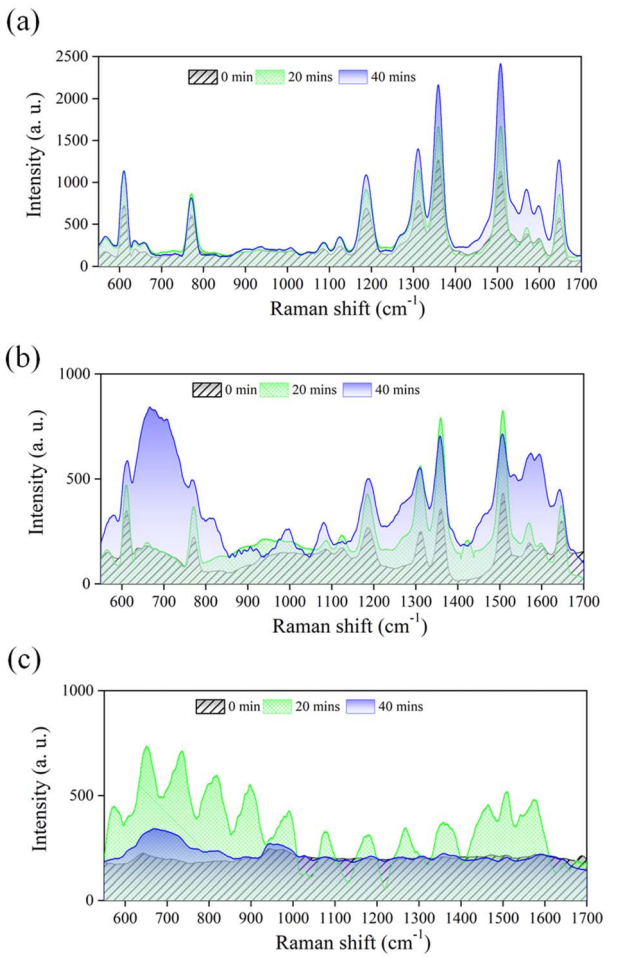

Fig. 5 Raman spectra of (a) 10^{-4} M, (b) 10^{-5} M, and (c) 10^{-6} M R6G on Au–TiO_2 decorated PSi substrates exposed to UV irradiation for different durations. All Raman spectra were obtained under the same conditions.

Future studies should optimize PIERS detection by altering the PLIP conditions, such as the concentrations of TiO_2 NPs and $HAuCl_4$ solution, employed in the fabrication of Au–TiO_2-decorated PSi substrates.

4. Conclusions

This study demonstrated the potential of Au/TiO_2-modified PSi fabricated through PLIP for use as a PIERS substrate. Unlike conventional-SERS substrates, such substrates utilize the large enhancement effect of UV irradiation on the analyte and require only short periods of irradiation for enhancement, particularly with higher analyte concentrations. Moreover, Au/TiO_2-modified PSi exhibits excellent stability and reproducibility for PIERS, providing a reliable measurement platform. Thus, we provide a new direction for PIERS advancement and a promising solution for Raman-based detection. In future research, we plan to optimize the performance of Au/TiO_2-modified PSi substrates and extend their application to other chemical and biological detection tasks.

Conflicts of interest

There are no conflicts to declare.

Acknowledgements

This research was funded by the project number MOST 110-2221-E-260-008-MY3 and TCVGH-NCNU-111-7902.

References

1 J. Plou, P. S. Valera, I. Garcia, C. D. L. de Albuquerque, A. Carracedo and L. M. Liz-Marzan, *ACS Photonics*, 2022, **9**, 333–350.
2 S. Pang, T. Yang and L. He, *TrAC, Trends Anal. Chem.*, 2016, **85**, 73–82.
3 Y. Qiu, C. Kuang, X. Liu and L. Tang, *Sensors*, 2022, **22**, 4889.
4 M. Fleischmann, P. J. Hendra and A. J. McQuillan, *Chem. Phys. Lett.*, 1974, **26**, 163.
5 J. Langer, D. Jimenez de Aberasturi, J. Aizpurua, R. A. Alvarez-Puebla, B. Auguie, J. J. Baumberg, G. C. Bazan, S. E. J. Bell, A. Boisen, A. G. Brolo, J. Choo, D. Cialla-May, V. Deckert, L. Fabris, K. Faulds, F. J. Garcia de Abajo, R. Goodacre, D. Graham, A. J. Haes, C. L. Haynes, C. Huck, T. Itoh, M. Kall, J. Kneipp, N. A. Kotov, H. Kuang, E. C. Le Ru, H. K. Lee, J. F. Li, X. Y. Ling, S. A. Maier, T. Mayerhofer, M. Moskovits, K. Murakoshi, J. M. Nam, S. Nie, Y. Ozaki, I. Pastoriza-Santos, J. Perez-Juste, J. Popp, A. Pucci, S. Reich, B. Ren, G. C. Schatz, T. Shegai, S. Schlucker, L. L. Tay, K. G. Thomas, Z. Q. Tian, R. P. Van Duyne, T. Vo-Dinh, Y. Wang, K. A. Willets, C. Xu, H. Xu, Y. Xu, Y. S. Yamamoto, B. Zhao and L. M. Liz-Marzan, *ACS Nano*, 2020, **14**, 28–117.
6 V. Shvalya, G. Filipič, J. Zavašnik, I. Abdulhalim and U. Cvelbar, *Appl. Phys. Rev.*, 2020, **7**, 031307.
7 G. Demirel, H. Usta, M. Yilmaz, M. Celik, H. A. Alidagi and F. Buyukserin, *J. Mater. Chem. C*, 2018, **6**, 5314–5335.
8 B. Tim, P. Blaszkiewicz and M. Kotkowiak, *Int. J. Mol. Sci.*, 2021, **23**, 291.
9 T. Y. Jeon, D. J. Kim, S. G. Park, S. H. Kim and D. H. Kim, *Nano Convergence*, 2016, **3**, 18.
10 M. Turino, N. Pazos-Perez, L. Guerrini and R. A. Alvarez-Puebla, *RSC Adv.*, 2021, **12**, 845–859.
11 C. Li, Y. Huang, X. Li, Y. Zhang, Q. Chen, Z. Ye, Z. Alqarni, S. E. J. Bell and Y. Xu, *J. Mater. Chem. C*, 2021, **9**, 11517–11552.
12 S. Ben-Jaber, W. J. Peveler, R. Quesada-Cabrera, E. Cortes, C. Sotelo-Vazquez, N. Abdul-Karim, S. A. Maier and I. P. Parkin, *Nat. Commun.*, 2016, **7**, 12189.
13 J. Zhao, Z. Wang, J. Lan, I. Khan, X. Ye, J. Wan, Y. Fei, S. Huang, S. Li and J. Kang, *Nanoscale*, 2021, **13**, 8707–8721.
14 M. Zhang, H. Sun, X. Chen, J. Yang, L. Shi, T. Chen, Y. Wu, Z. Bao and J. Liu, *ACS Sens.*, 2019, **4**, 1670–1681.
15 S. Almohammed, F. Zhang, B. J. Rodriguez and J. H. Rice, *Sci. Rep.*, 2018, **8**, 3880.
16 K. Abid, N. H. Belkhir, S. B. Jaber, R. Zribi, M. G. Donato, G. Di Marco, P. G. Gucciardi, G. Neri and R. Maâlej, *J. Phys. Chem. C*, 2020, **124**, 20350–20358.

17 Q. D. Mai, H. A. Nguyen, T. L. H. Phung, N. Xuan Dinh, Q. H. Tran, T. Q. Doan and A. T. Le, *ACS Appl. Nano Mater.*, 2022, **5**, 15518–15530.
18 H. Lin, J. Mock, D. Smith, T. Gao and M. J. Sailor, *J. Phys. Chem. B*, 2004, **108**, 11654–11659.
19 F. Giorgis, E. Descrovi, A. Chiodoni, E. Froner, M. Scarpa, A. Venturello and F. Geobaldo, *Appl. Surf. Sci.*, 2008, **254**, 7494–7497.
20 K. J. Khajehpour, T. Williams, L. Bourgeois and S. Adeloju, *Chem. Commun.*, 2012, **48**, 5349–5351.
21 A. Virga, P. Rivolo, F. Frascella, A. Angelini, E. Descrovi, F. Geobaldo and F. Giorgis, *J. Phys. Chem. C*, 2013, **117**, 20139–20145.
22 M. Kosovic, M. Balarin, M. Ivanda, V. Derek, M. Marcius, M. Ristic and O. Gamulin, *Appl. Spectrosc.*, 2015, **69**, 1417–1424.
23 H. Dridi, L. Haji and A. Moadhen, *Superlattices Microstruct.*, 2017, **104**, 266–270.
24 G. Demirel, H. Usta, M. Yilmaz, M. Celik, H. A. Alidagi and F. Buyukserin, *J. Mater. Chem. C*, 2018, **6**, 5314–5335.
25 I. Khalil, C.-M. Chou, K.-L. Tsai, S. Hsu, W. A. Yehye and V. K. S. Hsiao, *Appl. Sci.*, 2019, **9**, 4806.
26 B.-Y. Wang, Y.-S. Hsiao, P.-C. Wei, Y.-T. Liu, C.-C. Chu and V. K. S. Hsiao, *Catalysts*, 2022, **12**, 564.
27 N. Zhang, S. Q. Liu, X. Z. Fu and Y. J. Xu, *J. Phys. Chem. C*, 2011, **115**, 9136–9145.
28 H. Sun, J. T. He, Y. T. Wang, S. Y. Zhang, C. C. Liu, T. Sritharan, S. Mhaisalkar, M. Y. Han, D. Wang and H. Y. Chen, *J. Am. Chem. Soc.*, 2013, **135**, 9099–9110.